X-RAY OBSERVATIONS OF SN 1006 WITH *INTEGRAL*

E. Kalemci[1], S. P. Reynolds[2], S. E. Boggs[3], N. Lund[4], J. Chenevez[4], and M. Renaud[5]

[1]*Sabancı Universitesi, Orhanlı-Tuzla, İstanbul, 34956, Turkey.*
[2]*Department of Physics, NC State University, 2700 Stinson Drive, Box 8202, Raleigh, NC 27695, USA.*
[3]*Space Sciences Laboratory, 7 Gauss Way, University of California, Berkeley, CA, 94720-7450, USA.*
[4]*Danish National Space Center, Juliane Maries Vej 30, DK-2100 Copenhagen Ø, Denmark.*
[5]*Service d'Astrophysique, CEA-Saclay, 91191, Gif-Sur-Yvette, France*

ABSTRACT

We have used $\sim$1000 ksec of on-source, and 500 ksec of 10 degrees off-source *INTEGRAL* data of SN 1006 to characterize the synchrotron emission, and attempt to detect non-thermal bremsstrahlung, using the combination of IBIS and JEM-X spatial and spectral coverage. With the earlier 750 ksec on source data, we have detected the limbs of SN 1006 with JEM-X between 2.4 and 8.4 keV bands. The source was not detected with either ISGRI or SPI above 20 keV. The ISGRI upper limit is about a factor of four above current model predictions, but confirms the presence of steepening in the power-law extrapolated from lower energies (< 4 keV).

Key words: ISM:individual (SN1006), supernova remnants, X-rays:observations, radiation mechanisms:non-thermal.

1. INTRODUCTION

SN 1006 has been the prototype source for the study of electron acceleration to high energies in shocks. X-rays from this object were first reported by Winkler & Laird, 1976 [1]. *ASCA* observations showed that the limbs have featureless power-law spectra, whereas the interior has a thermal, line-dominated spectrum [2].

High energy electrons in supernova remnants (SNR) produce X-rays via non-thermal bremsstrahlung and synchrotron processes. In hard X-rays, synchrotron radiation from the tail of the electron distribution may compete with non-thermal bremsstrahlung from the very lowest-energy accelerated electrons. Electrons producing keV synchrotron emission could also produce very high-energy photons (in the TeV range) by IC upscattering of CMB photons [3]. A detection of the northeast (NE) limb of SN 1006 was reported in ground-based TeV observations by *CANGAROO-I* [4]. However, this result is later called into question by the observations of *H.E.S.S.*, and recent measurements by *CANGAROO-III* has also

claimed null result on SN 1006 [5]. Lower gamma-ray fluxes result in lower predicted bremsstrahlung flux by an order of magnitude. The nature of X-ray emission from SN 1006 above 10 keV is still uncertain. Below 10 keV, synchrotron emission should dominate. In principle, the *INTEGRAL* observatory can examine the effects of both the lowest and highest energy non-thermal electrons by distinguishing the synchrotron and bremsstrahlung emission with its imaging and spectral capabilities. The synchrotron emission should be concentrated in two bright opposing limbs like the radio emission, and should dominate the emission below 30 keV. The non-thermal bremsstrahlung will dominate at some energy between 30 and 300 keV [6].

Our group has observed SN 1006 for $\sim$1000 ks with the *INTEGRAL* Observatory [7] in AO-1 with the main aim of detecting and characterizing synchrotron emission, and distinguishing synchrotron and non-thermal bremsstrahlung emission by comparing the IBIS/ISGRI and JEM-X images to the model images. Later, in AO-3, an additional 2.5 MSec to SN 1006 was awarded, this time mainly to search for 511 keV emission from the source. The AO-3 observations were amalgamated with Cen X-4. The results of the AO-1 observations have already been published [8]. For AO-3, only the 10° offset data were available at the time of the workshop. Here, we summarize the AO-1 results and add the ISGRI results from AO-3.

2. OBSERVATIONS AND ANALYSIS

The *INTEGRAL* observations took place in three sets. The $\sim$250 ks first set ("Set I") was conducted early in the mission, between Jan, 11 and 20, 2003, corresponding to *INTEGRAL* revolutions 30 and 32. The $\sim$750 ks second set ("Set II") was conducted between Jan, 20 and 30, 2004, during revolutions 155-158. The third set ("Set III") is part of an amalgamation of SN 1006 and Cen X-4 and centered on on Cen X-4. It was conducted between Jan 29 and Feb 4 2006, corresponding to revolutions 402-404.

We did not use SPI (Spectrometer on *INTEGRAL* [9]), as ISGRI (see § 2.2 for more information) places much stricter limits in the hard X-ray band. Before the general analysis for all instruments, we filtered out the pointings with high Anti-Coincidence Shield rates, mostly occurring during the entry and exit of the radiation belts.

2.1. The JEM-X analysis

Set I, which was before a new background rejection criteria was implemented, was not included in this analysis. Set III was not used either as the central pointing of the dither pattern was 10 degrees away.

Although the total exposure for Set II is ∼750 ks, the effective exposure time of the central object is approximately 250 ks due to the vignetting of the JEM-X instrument during the 25 point dither. We have obtained JEM-X images in 2.4–4.2 keV, 4.2–8.4 keV, 8.4–14 keV, and 14–35 keV bands using the *JEM-X Midisky offline software package* [10]. The images from each pointing are then mosaicked using the *mosaic-weight* program [11]. These software were later implemented into OSA 5. The fluxes and the significance values shown in Table 1 are derived using the inner ASCA contours enclosing the NE and SW limbs to define two shape templates. The count excesses in the JEM-X mosaic images are then determined inside these two regions. The relevant noise figures are derived by defining a number of non-overlapping regions with the reference templates within a 60×60 pixel field (90×90 arc minutes) centered on SN1006. The statistical properties of the excess counts in these two sets of regions are used to derive RMS-noise of the background for regions of the two shapes. The fluxes are derived by comparing the excesses in the SN 1006 mosaics with corresponding excesses in mosaic images of the Crab Nebula obtained with the same INTEGRAL dither pattern, and correcting for the difference in the effective observation time.

2.2. The ISGRI analysis

The older background maps for Set I observations resulted in much noisier images compared to Set II images, and therefore we limit the analysis to the data from Set II and Set III. We used OSA 4.2 [12] standard programs for Set II and OSA 5.1 for Set III.

Since the ISGRI system point spread function is ∼13′, SN 1006 (∼30′ diameter) appears as an extended object to the imager. One needs to use simulations to obtain the effect of the extended nature of the source on the image and the measured flux. Such simulations have been conducted for ISGRI for different extended source geometries, including SN 1006 [13]. A reduction factor of 0.7 is obtained: that is, ISGRI would detect 70% of the true flux at each limb.
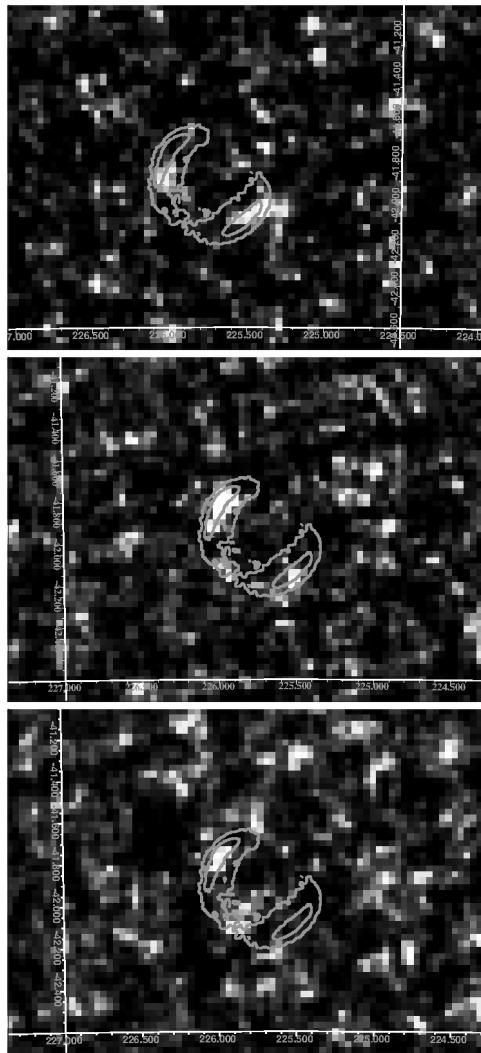

Figure 1. JEM-X reconstructed images of SN 1006 in three energy bands. Top: 2.4–4.2 keV, middle: 4.2–8.4 keV band, bottom: 8.4-14 keV. The ASCA *contours are overlaid. From Kalemci et al. [8]*

3. RESULTS

3.1. JEM-X results

The source is detected at the limbs in 2.4–4.2 keV and 4.2–8.4 keV bands (see Fig. 1 and Table 1). It appears that the South-West (SW) limb (the limb on the right in the images) is stronger in the 2.4–4.2 keV band at about the 1σ level, but the trend is reversed at higher energies. At 4.2–8.4 keV, the NE limb is stronger, a result with higher significance. An excess at the position of the NE limb is present in the 8.4–14 keV band ($1.7\,\sigma$), but no excess is seen in the SW limb. We note that *XMM-Newton* data also points to an asymmetry in flux coming from the NE and SW limbs such that the NE limb gets relatively stronger as energy increases [14]. A similar trend is seen in *ASCA* data [15], but the differences are small

North-East Limb Energy band (keV)	Flux $(10^{-4}$ phot/cm^{2}s)	Statistical significance	Model flux^a $(10^{-4}$ phot/cm^{2}s)
2.4–4.2^b	10 ± 4	2.6	14
4.2–8.4	11 ± 2	5.0	5.9
8.4–14	3.3 ± 1.9	1.7	1.4
South-West Limb			
2.4–4.2	15 ± 4	4.0	13
4.2–8.4	3.6 ± 2.3	1.6	4.8
8.4–14	<5.7	3^c	-

^{a}Flux from extrapolated model fit to the *ASCA* spectrum (0.8 - 9 keV), Dyer et al. 15

^{b}The actual low energy threshold is variable over different parts of the JEM-X detector.
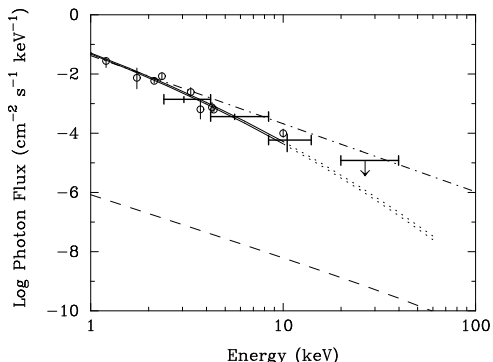
^{c}3σ upper limit

Figure 2. Integrated hard X-ray spectrum of SN 1006. The upper limit bar is from ISGRI. Open circles are pre-ASCA (see text) observations, and the two solid lines are the $\pm 1\sigma$ model fits to ASCA and RXTE data. The dotted-and-dashed line is the extrapolation from the Chandra spectral fit [19]. The dashed line is the bremsstrahlung prediction of the model described in text. The Set III results are not incorporated yet. From Kalemci et al. [8]

in the *ASCA* band (below 8 keV). The small excess of the SW over NE limbs in the 2.4–4.2 keV band we see is not supported by *ASCA* or *XMM-Newton* observations in that energy range.

Figure 2 shows our combined JEM-X fluxes for both limbs, compared with previous spatially integrated pre-*ASCA* flux measurements (see [16, 17] for references). The integrated fluxes have been converted to flux densities assuming a photon index Γ of 3.0 [18]. Also shown are a pair of model curves for the escape model that provided a good fit to *ASCA* and *RXTE* data [15]. The parameters of the best fit are a roll-off frequency of $\nu_{\rm roll} = 3.0 \times 10^{17}$ Hz and an electron energy index of 2.2 (implying a radio spectral index $\alpha = 0.6$ or radio photon index $\Gamma \equiv \alpha + 1 = 1.6$). These parameters imply an e-folding energy of the exponential cutoff (due to escape) of $32(B_2/10\mu{\rm Gauss})^{-1/2}$ TeV (where B_2 is the post-shock field). The curves in Figure 2 correspond to $\pm 1\sigma$ errors on $\nu_{\rm roll}$: $(2.8 - 3.1) \times 10^{17}$ Hz. The dashed line indicates the bremsstrahlung prediction for an upstream density of 0.2 cm^{-3} and $B_2 = 10\mu$Gauss.

3.2. ISGRI results

We obtained ISGRI images in different energy bands using OSA 4.2 for Sets I and II, and OSA 5.1 for Set III. The Sets have not been merged yet. SN 1006 was not detected in any band. The 20-40 keV sigma images for set II and III are shown in Fig. 3. The 3 σ upper limit (sensitivity limit) for a point source for $\sim$750 ks observing time is $\sim 9 \times 10^{-5}$ photon cm^{-2} s^{-1}. If synchrotron dominates in 20–40 keV band, the emission would be concentrated in two limbs. The extended nature of the source causes a reduction factor of 0.7 in flux (see § 2.2). Therefore the 3 σ upper limit for a synchrotron dominated source is 1.3×10^{-4} photon cm^{-2} s^{-1} at each limb. For synchrotron dominated emission, the expected total flux in the 20–40 keV band (based on the models shown in Figure 2) is $(2.9 - 3.6) \times 10^{-5}$ photon cm^{-2} s^{-1} for the entire remnant, or roughly half this at each limb. The bremsstrahlung emission from the model shown in Figure 2, using the lower-limit 25 μG downstream magnetic field from *H.E.S.S.* TeV observations, is predicted to be about 2×10^{-8} photon cm^{-2} s^{-1}, far below ISGRI's sensitivity. In fact, in this case, since the emission would be coming from a larger area, the upper limit set by our observations is even higher. The predicted crossover energy where bremsstrahlung and synchrotron emission become comparable is in the vicinity of 200 keV.

Long et al. (2003) reported that a power-law photon index of 2.30 fit the Chandra data well between 0.5 and 5 keV for the emission at the limbs. An extrapolation of this fit from 5 keV to the ISGRI range is also shown in Fig. 2 with a dotted-and-dashed line. Our ISGRI upper limit is about a factor of 2 below the extrapolation of this power-law to 28 keV.

4. DISCUSSION

Coded-mask imaging is a complex process, and optimal techniques are still being developed to clean noisy images, both for JEM-X and ISGRI. Our results confirm and extend results obtained with *ASCA*, *Chandra X-ray Observatory*, and *XMM-Newton*, and show that relatively small increases in sensitivity may allow ISGRI to detect predicted synchrotron radiation for some models.

The prospect of detecting bremsstrahlung X-rays or gamma-rays from SN 1006 has become considerably more remote with the combination of lower estimates for the ambient density and the much higher magnetic field that would be required to explain the lack of IC from CMB photons in the *H.E.S.S.* observations. However, it is quite possible that *INTEGRAL* observations conducted during Cycle 3 will have sufficient sensitivity to detect synchrotron emission in the 18-40 keV band. A model that can describe the observations of Figure 2 but with a strong enough magnetic field to satisfy the *H.E.S.S.* constraints (downstream $B > 25\mu$G) is somewhat harder than the spectra shown in Figure 2, and predicts a flux

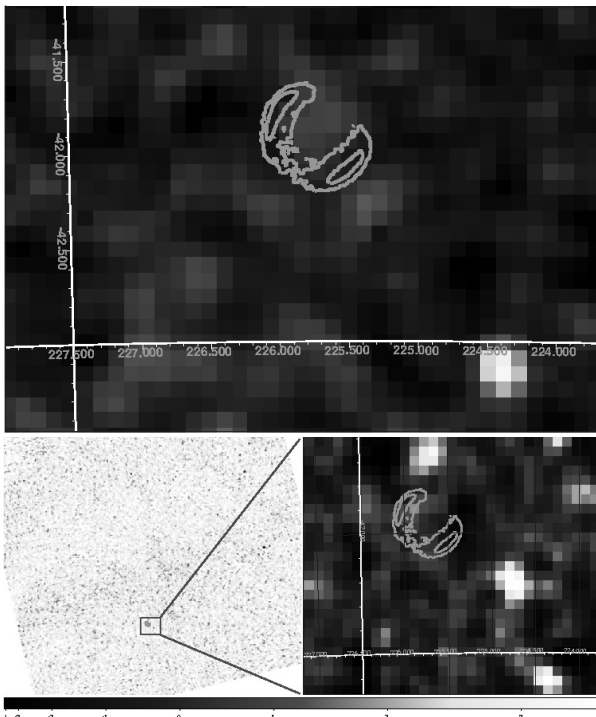*Figure 3. Top: The ISGRI sigma image around SN 1006 in 20–40 keV band for Set II. SN 1006 is not detected. A nearby source [VV 780, 11.6 σ detection 20] is also shown for comparison. The ASCA contours are overlaid to show the expected position of SN 1006. The feature at the center of SN 1006 is not significant, and is possibly due to inaccurate background map. Bottom left: ISGRI 20-40 keV image using Set III, showing offset. Bottom right: Set III, close to SN 1006. VV 780 with 4.2 σ is the brightest source.*

in the 18-40 keV band of 0.3×10^{-4} photon cm^{-2} s^{-1}. Some models predict considerably lower fluxes in the 18–40 keV band, so ISGRI detection would not only extend and confirm the presence of hard synchrotron X-rays, but could provide useful model discrimination.

We have obtained the first observations with JEM-X of an extended source, between 2.4 and 14 keV. The fluxes we derive are consistent with those of earlier imaging observations where they overlap, and support the identification of the continuum emission of SN 1006 as synchrotron radiation from a slowly dropping off electron distribution. Our ISGRI 3σ upper limit is about a factor of 4 higher than the prediction of the model that best fits the soft X-ray continuum. With ISGRI, we confirm at higher energies than has been previously reported that the X-ray spectrum of SN 1006 must be steepening. The results from the new datasets for both ISGRI and JEM-X will be included in the analysis in the near future.

REFERENCES

[1] Winkler, P. F. & Laird, F. N. 1976, ApJ, 204, L111

[2] Koyama, K., Petre, R., Gotthelf, E. V., et al. 1995, Nature, 378, 255

[3] Pohl, M. 1996, A&A, 307, L57

[4] Tanimori, T. & et al. 1998, ApJ, 497, 25

[5] Tanimori, T. & et al. 2005, in International Cosmic Ray Conference, 215–+

[6] Reynolds, S. P. 1999, Astrophys. Lett. Commun., 38, 425

[7] Winkler, C., Courvoisier, T. J.-L., Di Cocco, G., et al. 2003, A&A, 411, L1

[8] Kalemci, E., Reynolds, S. P., Boggs, S. E., et al. 2006, ApJ, 644

[9] Vedrenne, G., Roques, J.-P., Schönfelder, V., et al. 2003, A&A, 411, L63

[10] Lund, N., Westergaard, N. J., Budtz-Joergensen, C., et al. 2004, in Proc. of The 5th INTEGRAL Workshop, The INTEGRAL Universe, Munich, 16-20 Feb. 2004

[11] Chenevez, J., Lund, N., Westergaard, N. J., et al. 2004, to appear in: Proc. of The 5th INTEGRAL Workshop, The INTEGRAL Universe, Munich, 16-20 Feb. 2004, astro-ph/0406682

[12] Goldwurm, A., David, P., Foschini, L., et al. 2003, A&A, 411, L223

[13] Renaud, M., Lebrun, F., Terrier, R., Reynolds, S. P., & Kalemci, E. 2006, A&A, 456,389

[14] Rothenflug, R., Ballet, J., Dubner, G., et al. 2004, A&A, 425, 121

[15] Dyer, K. K., Reynolds, S. P., & Borkowski, K. J. 2004, ApJ, 600, 752

[16] Reynolds, S. P. 1996, ApJ, 459, L13

[17] Hamilton, A. J. S., Sarazin, C. L., & Szymkowiak, A. E. 1986, ApJ, 300, 698

[18] Allen, G. E., Petre, R., & Gotthelf, E. V. 2001, ApJ, 558, 739

[19] Long, K. S., Reynolds, S. P., Raymond, J. C., et al. 2003, ApJ, 586, 1162

[20] Kalemci, E., Boggs, S. E., & Lund, N. 2005, The Astronomer's Telegram, 410